ARL-TR-10407 ● AUG 2026

Oriented Morphologies in 2D Polymer Films

by Frederick L. Beyer, Noah J. Zahn, David C. McLeod,
Emil Sandoz-Rosado, and Eric D. Wetzel

NOTICES

Disclaimers

The findings in this report are not to be construed as an official Department of the Army position unless so designated by other authorized documents.

Citation of manufacturer's or trade names does not constitute an official endorsement or approval of the use thereof.

Destroy this report when it is no longer needed. Do not return it to the originator.

ARL-TR-10407 ● AUG 2026

Oriented Morphologies in 2D Polymer Films

Frederick L. Beyer, Noah J. Zahn, David C. McLeod,
Emil Sandoz-Rosado, and Eric D. Wetzel
DEVCOM Army Research Laboratory

REPORT DOCUMENTATION PAGE

1. REPORT DATE	2. REPORT TYPE	3. DATES COVERED	
		START DATE	END DATE
August 2026	Technical Report	10/1/2024	9/30/2025

4. TITLE AND SUBTITLE
Oriented Morphologies in 2D Polymer Films

5a. CONTRACT NUMBER	5b. GRANT NUMBER	5c. PROGRAM ELEMENT NUMBER
5d. PROJECT NUMBER	**5e. TASK NUMBER**	**5f. WORK UNIT NUMBER**

6. AUTHOR(S)
Frederick L. Beyer, Noah J. Zahn, David C. McLeod, Emil Sandoz-Rosado, and Eric D. Wetzel

7. PERFORMING ORGANIZATION NAME(S) AND ADDRESS(ES)	8. PERFORMING ORGANIZATION REPORT NUMBER
DEVCOM Army Research Laboratory ATTN: FCDD-RLA-MG Aberdeen Proving Ground, MD 21005	ARL-TR-10407

9. SPONSORING/MONITORING AGENCY NAME(S) AND ADDRESS(ES)	10. SPONSOR/MONITOR'S ACRONYM(S)	11. SPONSOR/MONITOR'S REPORT NUMBER(S)

12. DISTRIBUTION/AVAILABILITY STATEMENT
DISTRIBUTION STATEMENT A. Approved for public release: distribution unlimited.

13. SUPPLEMENTARY NOTES
ORCIDs: Frederick L. Beyer, 0000-0003-0253-2134; Noah J. Zahn, 0009-0005-8040-1270; David C. McLeod, 0000-0001-5293-6060; Emil Sandoz-Rosado, 0000-0002-9587-2738; Eric D. Wetzel, 0000-0002-0176-3072

14. ABSTRACT
Covalent organic frameworks, also called two-dimensional polymers (2DPs), are of interest for several reasons, including theoretical strength, very high porosity, and high degree of anisotropy. In this work, 2DPs were synthesized from 1,3,6,8-tetrakis(4-aminophenyl)pyrene (TAPPy) and terephthalaldehyde (PDA), and then cast onto oriented substrates to test the ability of the substrate to induce macroscopic orientation in the resulting 2DP films. Using wide-angle X-ray scattering, it was shown that the 2DP molecules possessed a high degree of orientation within the films. The degree of orientation, size, and shape of the 2DP stacks and effects of chemical functionality (imine vs. amide) were analyzed.

15. SUBJECT TERMS
Sciences of Extreme Materials, two-dimensional polymers, covalent-organic framework, morphology, X-ray scattering, small-angle X-ray scattering, SAXS, wide-angle X-ray scattering WAXS, TAPPy-PDA

16. SECURITY CLASSIFICATION OF:			17. LIMITATION OF ABSTRACT	18. NUMBER OF PAGES
a. REPORT	b. ABSTRACT	C. THIS PAGE		
UNCLASSIFIED	UNCLASSIFIED	UNCLASSIFIED	UU	37

19a. NAME OF RESPONSIBLE PERSON	19b. PHONE NUMBER *(Include area code)*
Frederick L. Beyer	(520) 691-5214

STANDARD FORM 298 (REV. 5/2020)
Prescribed by ANSI Std. Z39.18

Contents

List of Figures

List of Tables

Acknowledgments

Mr. Noah Zahn conducted research on this project as an ARL Research Associateship Program participant. He was funded via the award of cooperative agreement, W911NF-24-2-0169.

1. Introduction

Covalent organic frameworks (COFs) are large, planar molecules formed by the reaction of reagents having well-defined, planar structures such that large network lattice is formed during polymerization.[1] At the most basic level, COFs are formed by the reaction of two monomers (A and B) having molecular symmetry such that a planar lattice, rather than a linear chain, is produced.[2] In Figure 1, which illustrates the lattice structure of the materials in this study, monomer A has tetragonal symmetry and four reactive groups while monomer B is linear with two reactive groups. Reaction of these monomers leads to the formation of large, flat molecules, commonly called two-dimensional polymers (2DPs). Evans et al.[3] defined 2DPs as molecules that are topologically planar, covalently linked, and molecularly thin.

In this study, 2DPs were synthesized from 1,3,6,8-tetrakis(4-aminophenyl)pyrene (TAPPy) and terephthalaldehyde (PDA). As illustrated in Figure 1, the reaction of TAPPy and PDA leads to the formation of a 2DP with a roughly "square" lattice structure. The individual 2DP molecules are sheet-like in their shape. Due to attractive intermolecular interactions, the molecules tend to form stacks analogous to tactoids in clay minerals.[4] Due to the many similarities between clay tactoids and stacks of 2DP molecules, in this work the stacks will also be called tactoids.

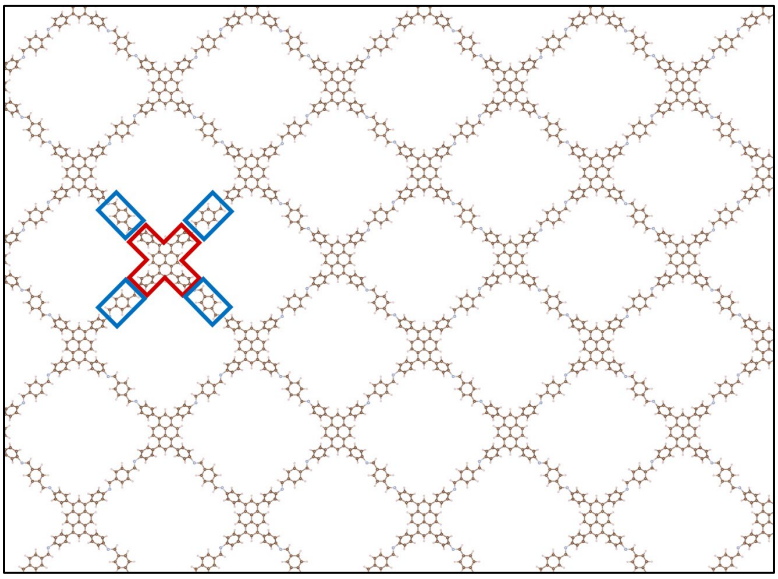

Figure 1. Illustration of TAPPy-PDA molecular structure with tetrafunctional TAPPy highlighted in red and difunctional PDA highlighted in blue.

A key goal of the U.S. Army Combat Capabilities Development Command (DEVCOM) Army Research Laboratory's (ARL's) research in 2DPs is the formation of bulk materials in which the 2DP molecules are aligned over macroscopic length scales. It is hypothesized that macroscopic alignment of 2DPs

in a bulk material will lead to mechanical and physical properties that reflect the large-scale and redundant covalent chemical network formed at the molecular level. This study explores the effect of TAPPy-PDA synthesis and of templating using oriented substrates during the film casting process on morphology and particularly on the development of morphological orientation.

2. Experimental Materials and Methods

2.1 Materials Synthesis and Processing

All the TAPPy-PDA imine samples were made as follows: 0.938 g of benzoic acid was dissolved in 4.43 mL of benzonitrile with 0.59 mL of water (corresponding to 9 vol% of the total solution) at 90 °C in a 20-mL scintillation vial. Once heated, 0.5 mL of a 24 mg/mL solution of PDA in benzonitrile was added, followed quickly by 0.57 mL of a 0.7 M solution of aniline in benzonitrile (1 equivalent of aniline per aldehyde). This mixture was heated for 30 s and then 0.5 mL of a 56 mg/mL solution of TAPPy was added (total volume = 6 mL, 1.1 equivalent of amine per aldehyde). The mixture was heated for 2 h and then transferred to an ice bath at 0 °C. Dissolved benzoic acid was allowed to crystallize from solution for 30 min. After the benzoic acid was crystallized, 10 mL of methanol was added and the solution shaken until the benzoic acid was dissolved, leaving only orange TAPPy-PDA solids remaining. The resulting precipitates were filtered out using vacuum filtration or a tea bag, then added to an ethanol bath for a minimum of 18 h. After the ethanol bath, the samples were died in supercritical CO_2 and collected, producing a solid powder of flake-shaped particles.

The flakes of TAPPy-PDA were dissolved in various solvents including 1,4-dioxane and tetrahydrofuran (THF) at a concentration of 4 mg/mL before being cast as large area films (~64 cm^2) on various substrates. Substrates included a hexavalent chromium-coated aluminum panel, filter paper, and graphite. The films were very thin and sometimes delaminated spontaneously from the substrate. They demonstrated electrostatic characteristics. They were relatively strong, given their thickness, but could be torn easily.

In this report, samples are denoted as described in Table 1, with sample names indicating overall chemistry, functionalization (imine vs. amide), concentration in casting solvent, and casting substrate.

Table 1. Sample characteristics and nomenclature.

Sample	Notebook reference	Functionality	Concentration (mg/mL)	Solvent	Substrate
TP-I-DOX-AL	NZ-2-8-I	Imine	4	Dioxane	Cr(VI)-coated Al
TP-I-DOX-GR	NZ-2-42-I	Imine	7	Dioxane	Graphite
TP-I-THF-GR	NZ-2-45-I	Imine	6	THF	Graphite
TP-A-DOX-FP	NZ-2-25-2-A	Amide	10	Dioxane	Filter paper
TP-A-DOX-GR	NZ-2-42-6-A	Amide	10	Dioxane	Graphite
TP-A-THF-GR	NZ-2-45-A	Amide	10	THF	Graphite

Sample TP-I-DOX-AL was fabricated by dissolving flakes of TAPPy-PDA in 1,4 dioxane at a concentration of 4 mg/mL, followed by solvent casting as large area films (~10 inches^2) on a hexavalent chromium-coated aluminum panel. These films were very thin, would delaminate spontaneously from the substrate, and were highly electrostatic. They were impressively strong for films of their thickness but could be torn with minimal effort.

Sample TP-I-DOX-GR was cast from a 7-mg/mL solution of TAPPy-PDA flakes in dioxane. A strongly cohesive coating was created when the solution was cast on graphite. The coating could be delaminated via submersion in water to produce a free-standing film.

Sample TP-I-THF-GR was created by dispersing TAPPy-PDA flakes in THF. Films of TAPPy-PDA flakes in THF could not be cast from dispersions exceeding a concentration of 6 mg/mL. The solution did not wet graphite substrates. When cast on filter paper, the solution formed a continuous film, which did not have a smooth surface and delaminated spontaneously when dunked in water and left to air dry.

All of the TAPPy-PDA amide flakes were made as follows: 60 mg of flakes of the TAPPy-PDA imine were added to 96 mg of potassium peroxymonosulfate (also known as “oxone”), 45 mL of N,N-dimethylformamide (DMF), 0.24 mL of acetic acid in a 20-mL vial and stirred overnight at room temperature. The resulting TAPPy-PDA was amidized, washed with water, washed with THF, soaked in methanol overnight, soaked in hexane for 1 h, and then supercritical CO_2 dried. The resulting powder was suspended in either dioxane or THF at 10 mg/mL. For both dioxane and THF suspensions, filter paper and graphite substrates formed high-quality freestanding films.

2.2 Wide-Angle X-ray Scattering

Wide-angle X-ray scattering (WAXS) data were collected using a Xenocs Xeuss 3.0 HR camera with X-rays generated by a Rigaku MicroMax 007HF rotating

anode source operated at 1.2 kW with a copper anode. The resulting photons were monochromated and filtered with a focusing optic such that wavelength (λ) was 1.542 Å (Cu-Kα). Incident beam collimation was by two apertures comprising slit optics, where the second aperture had scatterless slits. In most experiments, the slit openings were 0.6 mm for the upstream aperture and 0.4 mm for the downstream aperture. Scattered intensity was measured using a Dectris PilatusR 300K solid-state detector. The sample-to-detector distance was set to 140 mm so that the detector covered an effective angular range of q = 0.1 to 2.0 Å^{-1}, where q is the scattering vector magnitude, $q = (4\pi \sin\theta)/\lambda$, and 2θ is the scattering angle. For Cu-Kα photons, this angular range corresponds roughly to 1.5–28 °2θ. The sample-to-detector distance and beam center were both calibrated with NIST Standard Reference Material LaB_6.[5]

Data processing, correction, and analysis were performed using Wavemetrics Igor Pro software and procedures developed at Argonne National Laboratory (Lamont, Illinois).[6,7] When the scattered data were isotropic, 2D data were converted to 1D form by azimuthal averaging, including corrections for spatial distortions caused by the projection of spherical scattering onto a planar surface.[8] Where possible, data were placed on an absolute scale using transmitted flux and sample thickness. Analysis of the crystal structure was performed using standard methods.[9] Structure visualization and model diffraction patterns were generated using VESTA 3.90.5a.[10]

2.3 Sample Rotation Experiments

Collection of WAXS data from rotated samples was performed using a rotation stage and a purpose-made sample holder. Sample rotation was about the instrument *z*-axis, which is the vertical direction in the laboratory. In a standard transmission-geometry experiment, a piece of sample in film format is placed on a sample holder so that the incident X-ray beam is normal to the plane of the film. Rotation of the sample about the *z*-axis reduces the angle of incidence from 90° (transmission) to 0° (in-plane). In this report, the data are designated by the angle of rotation (Ω) rather than the angle of incidence, such that Ω = 0° corresponds to transmission while Ω = 90° indicates that the X-ray beam is parallel to the plane of the film. The sample holder, illustrated in Figure 2, includes a horizontal channel that allows the sample to be rotated fully to Ω = 90° without the holder impinging on the incident beam or scattered photons.

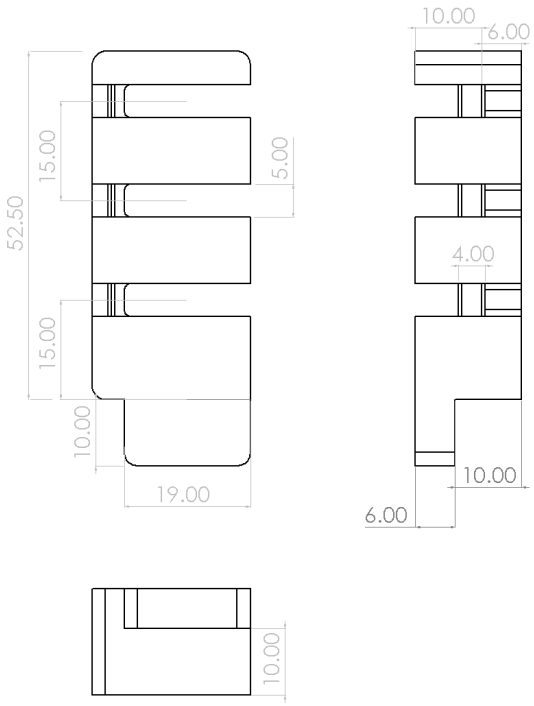

Figure 2. Technical drawing of a sample holder allowing rotation of samples about the instrument *z*-axis. All dimensions are in millimeters.

2.4 Stacking Peak Analysis

Analysis of the (001) diffraction peak, also called the stacking peak, was accomplished by fitting the azimuthally averaged X-ray diffraction data with a Lorentz distribution. To accurately determine the center of the peak (q_0), a linear background and a constant background were also fit to the data, as given in Equation 1. Equation 1 also includes a second Lorentz distribution, which was necessary to correctly fit the stacking peak for samples cast on graphite. In Equation 1, A_i is the peak amplitude, q_i is the peak center, γ_i is the peak half-width at half-maximum, m is the slope of the linear background, and I_0 is the constant background value.

$$I(q) = \frac{A_0}{\pi}\left(\frac{\gamma_0}{(q-q_0)^2+{\gamma_0}^2}\right) + \frac{A_1}{\pi}\left(\frac{\gamma_1}{(q-q_1)^2+{\gamma_1}^2}\right) + mq + I_0 \qquad (1)$$

2.5 Domain Size Analysis

The Scherrer equation allows the estimation of crystal size from diffraction data.[9,11] As given in Equation 2, the grain size (τ) is a function of a constant (K), λ, the full-width at half-maximum (FWHM) (β) of the diffraction peak in question, and the Bragg angle (θ) of the diffraction peak. In general, the value of K is taken as 0.9,

although this varies somewhat with application.[11] When using the Lorentz distribution, $\beta = 2\gamma$.

$$\tau = \frac{K\lambda}{\beta \cos\theta} \tag{2}$$

2.6 Orientation Analysis

The Herman's orientation function describes the orientation of a diffraction peak relative to a reference direction.[12] As given in Equation 3, the Herman's orientation parameter, f, is defined so that when φ, the average angle between the preferred direction and the normal of the diffraction plane, is 0°, the value of f is 1. When the orientation is perfectly normal to the desired direction, $\varphi = 90°$ and $f = -½$. For perfectly random orientation, the function returns $f = 0$.

$$f = \frac{3\langle cos^2\,\varphi\rangle - 1}{2} \tag{3}$$

3. Results

3.1 Crystal Structure

A prior study by Natraj et al.[13] determined that the crystal structure of TAPPy-PDA COFs is monoclinic with C2/*m* symmetry, dimensions a = 32.545 Å, b = 34.286 Å, c = 3.846 Å, and unit cell angles of $\alpha = \beta = 90°$, and γ = 85.371°.* The 2D structure of TAPPy-PDA and the unit cell are illustrated in Figure 3. These parameters were used to calculate the distance between lattice planes (*d*-spacing) for allowed reflections for the monoclinic structure and compared directly to the experimental 1D data for peak identification. Because TAPPy-PDA forms a planar structure, the monoclinic unit cell in the *c*-direction corresponds to direction normal to the TAPPy-PDA planar molecule, the distance between molecules is c, and the (001) reflection is the stacking peak.

*Natraj et al.[13] report that β = 85.371° and γ = 90°, but this appears to be in error as the structure analysis fails unless γ = 85.371° and β = 90°.

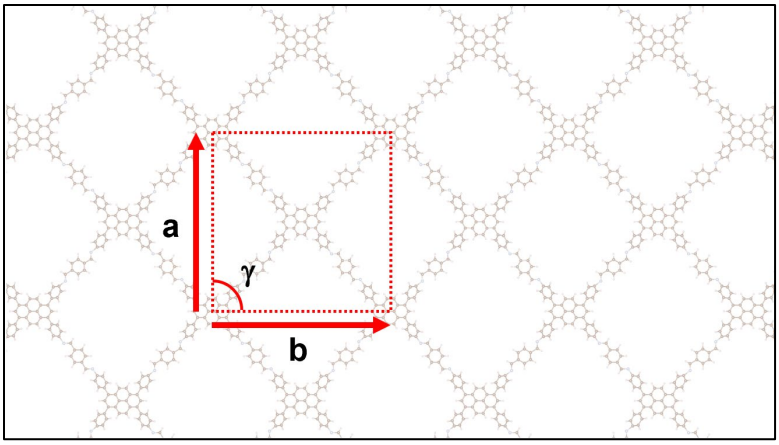

Figure 3. Illustration of TAPPy-PDA molecular structure viewed normal to the molecular plane. The monoclinic C2/*m* unit cell is illustrated in red, with crystallographic axes a and b and crystallographic angle γ labeled.

Figure 4 shows an example of the X-ray diffraction data collected for the TAPPy-PDA samples in this study. At least 8 diffraction peaks can be visually identified in Figure 4 and closer scrutiny reveals that two of the larger peaks are combinations of at least two distinct peaks. Using the monoclinic C2/*m* structure and unit cell parameters given above, diffraction peaks were identified for the (110), (200), (220), (310), (330), (420), (150), (440), (350), and (550) planes, as shown in Figure 4. All diffraction peaks were fit with Lorentzian distributions. The low-q upturn was fit using a power law of the form $I(q) \propto q^{-p}$, where p is the power law exponent. A constant background was also used. The peak for (550) was not fit due to the limitations of the Irena software package.[6]

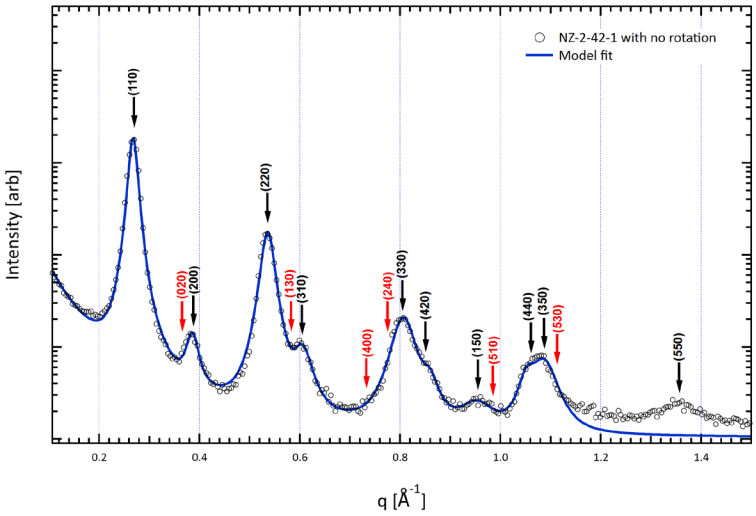

Figure 4. X-ray scattering data and results of diffraction modeling for sample TP-I-DOX-GR. Diffraction peaks are indicated by black (observed) and red (not observed) arrows.

The extinction rule for the monoclinic C2/*m* structure is observation of diffraction peaks only for planes with $h + k = 2n$, where *n* is an integer. Therefore, diffraction is also expected from the (020), (130), (040), (400), (240), (510), and (530) planes. The predicted positions of these diffraction peaks are identified by the red arrows in Figure 4. Their absence from the scattering data can be explained by the effect of the shape of the scattering domains through the concept of the form factor.

The measured X-ray scattering from two-phase materials is the convolution of scattering from a function describing the shape of the minority component and the scattering from the organization of the minority component.[14] The shape function is called a form factor, $P(q)$, and the organization function is called the structure factor, $S(q)$. Equation 4 describes this relationship.

$$I(q) \propto P(q) * S(q) \tag{4}$$

When the concentration of scattering objects is diluted, only form factor scattering is observed (i.e., $S(q) = 1$). As the objects become more concentrated, inter-particle interference begins and the structure factor begins to affect the observed scattering. In this concentration region, the first correlation peak occurs. As the concentration of domains continues to increase, packing into an organized structure is often observed, such as in the case of low-polydispersity block copolymers. The observed scattering is then often dominated by the structure factor. The convolution of the structure factor with the form factor then effectively eliminates specific diffraction peaks, where those peaks would be observed at the same angle as a minimum in the form factor. Although wide-angle diffraction is generally not considered in terms of a structure factor and a form factor, this approach is valid in both the small- and wide-angle regimes.

As noted previously, the effective morphology in well-ordered 2DP tactoids is one of columnar voids in an organic matrix.[15] In Figure 5, the form factor for cylindrical objects 200 Å in length and 20 Å in diameter is shown in blue. The minima in the form factor occur at regular intervals. Figure 5 also shows the calculated diffraction peaks for a model compound having the monoclinic C2/*m* structure with the same lattice parameters as TAPPy-PDA (red trace). The gray bands illustrate the angular regions in which the form factor will reduce or eliminate specific allowed reflections. One can see that these regions correspond well to the regions of low intensity in the observed data for TP-I-THF-GR, confirming the presence of voids with an approximately cylindrical structure, as expected for stacks to TAPPy-PDA 2DPs.

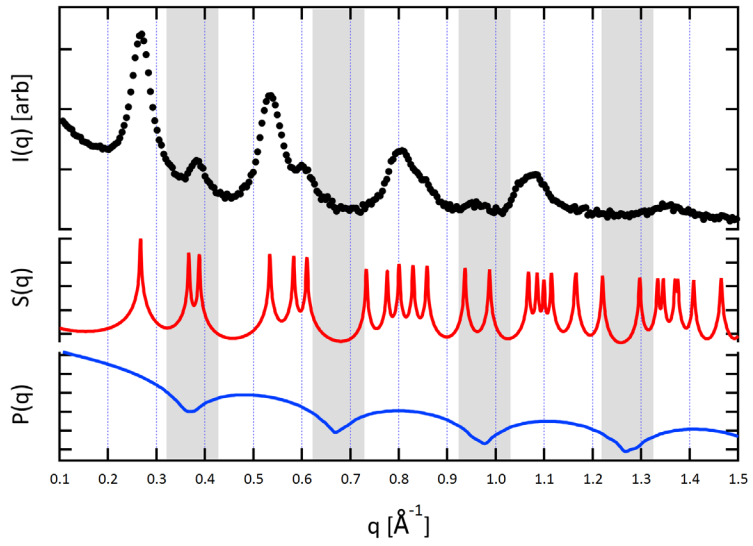

Figure 5. Comparison of the measured scattering data from TP-I-DOX-GR (black circles) with the form factor scattering (blue line) from a cylinder 200 Å long and 20 Å in diameter, and the predicted diffraction peaks (red line) from a simple compound having the same unit cell as TAPPy-PDA COFs. The shaded regions illustrate the effect of form factor minima in the overall diffraction pattern.

Figure 6 shows the X-ray diffraction data collected for the six COFs in this study. The data, which have been offset for clarity, confirm that all six have the expected TAPPy-PDA structure. Sample TP-I-DOX-AL (2-8-I) (black) is well-ordered, with four large and at least two smaller diffraction maxima. Samples TP-I-THF-GR (2-45-I) (blue) and TP-I-DOX-GR (2-42-6-I) (purple) are both very well-ordered, with four large diffraction maxima, but also six weaker maxima extending to high angles. Sample TP-A-DOX-FP (2-25-2-A) (green) is comparable to TP-I-DOX-AL (2-8-I), with good crystalline order, but samples TP-A-DOX-GR (2-42-6-A) (orange) and TP-A-THF-GR (2-45-A) (red) decreased ordering. The weak peak at approximately 1.68 $Å^{-1}$ for samples TP-I-THF-GR (2-45-I) and TP-I-DOX-GR (2-42-6-I) is most likely due to regular stacking of the molecular sheets (the "stacking peak"). Based on the Natraj crystal structure,[13] the (001) peak should be observed at 1.64 $Å^{-1}$. The other most likely diffraction peak in this range is the (660) peak, which would be observed at 1.60 $Å^{-1}$.

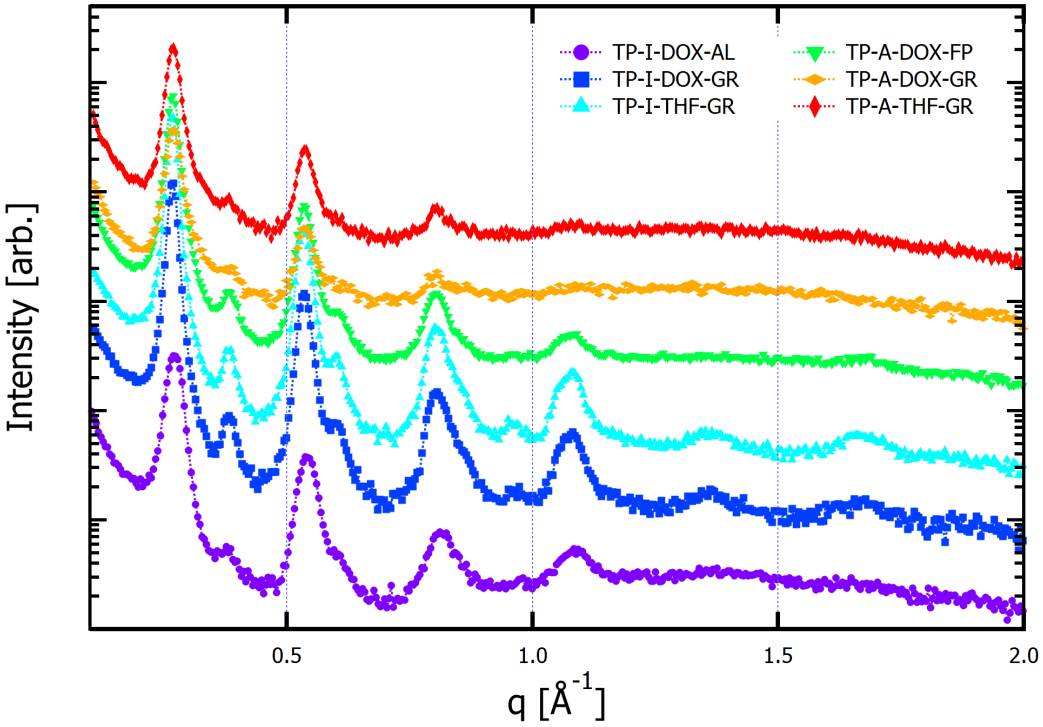

Figure 6. Diffraction data for the six samples in this study, collected with no sample rotation. Data are offset vertically for clarity. Intensity is on a logarithmic scale.

3.2 Orientation

Rotating sample TP-I-DOX-AL about the *z*-axis caused a remarkable change in the scattering data. As shown in Figure 7, the scattering pattern changed from one of isotropic orientation with little evidence of stacking (Figure 7A) to one of highly anisotropic scattering with a strong stacking peak (Figure 7B). This change clearly indicates that the stacks of TAPPy-PDA 2D molecules are themselves oriented such that the molecular sheets lie predominantly in the plane of the film. Figure 7C shows the resulting 1D scattering data for TP-I-DOX-AL for every 10° increment in Ω. The stacking peak at 1.7 $Å^{-1}$ generally increases in intensity with increasing rotation because of the preferred orientation. However, close inspection reveals that the data at Ω = 90° have a lower overall intensity than that collected at Ω = 80°. This is caused by small tears and wrinkles in the sample, defects that cause changes in the volume of material in the X-ray beam. Because measured intensity is directly proportional to the volume of sample interrogated, changes in the volume of sample in the beam cause linear changes in measured intensity.[12] Even in smooth films, rotation about the *z*-axis increases the sample volume in the beam, as can be seen in the increase in background intensity as the sample is rotated to progressively higher Ω.

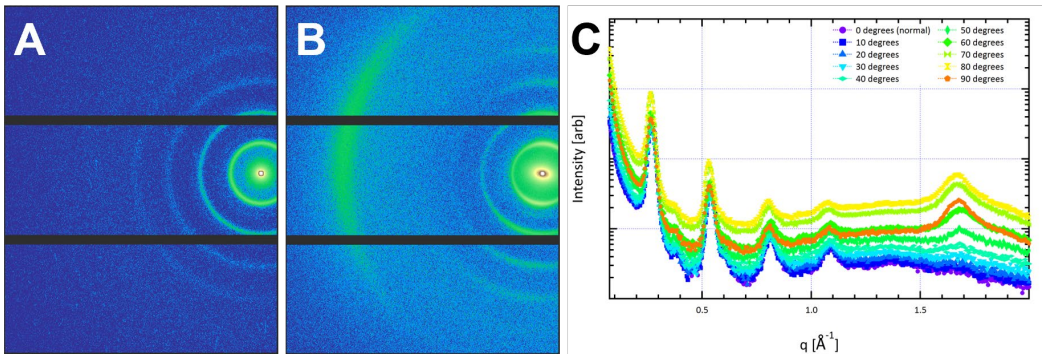

Figure 7. X-ray scattering data collected for sample TP-I-DOX-AL: A) 2D data at Ω = 0°, B) 2D data at Ω = 90°, and C) 1D data after azimuthal averaging.

The effect of changing sample volume can be largely removed from the data by normalizing the data in a region of q where there is little (or constant) structural information. In this case, the data can be normalized by the intensity at $q < 0.15$ Å^{-1}, where $I(q)$ exhibits power law behavior due to large-scale, isotropic morphological features (e.g., surface texture, Guinier scatter, and so on). Figure 8 shows the same 1D data after normalization, showing that the increase in the stacking peak intensity is mostly due to rotation and morphological anisotropy.

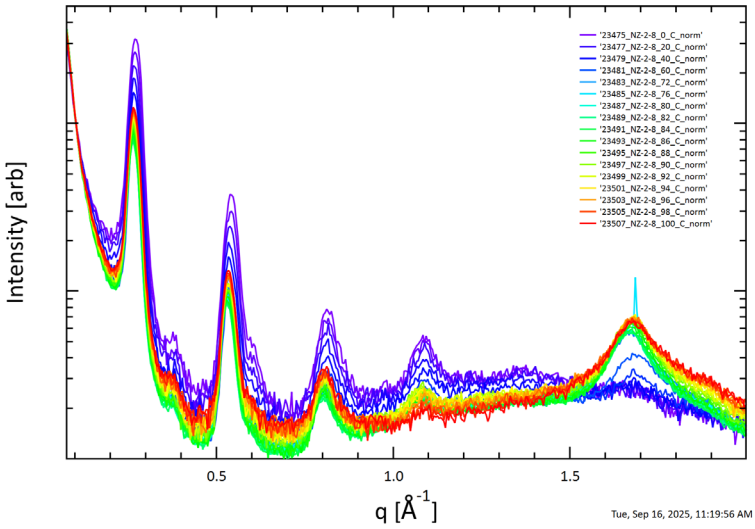

Figure 8. 1D scattering data for sample TP-I-DOX-AL at different Ω, normalized by the scattered intensity at $q < 0.15$ Å^{-1}, revealing the sudden onset of diffraction from the stacking peak around Ω = 70°.

The increase in intensity at $q \approx 1.68$ Å^{-1} also eliminates the possibility that the peak is of the form (hk0), such as that predicted for (660). In Figure 8, the other diffraction maxima all decrease in intensity with increasing Ω. This behavior is opposite that of the stacking peak.

To correctly determine the spacing between TAPPy-PDA layers in these materials, the stacking peak was fit with a Lorentz distribution. The stacking peak is superimposed on very weak background scattering from the amorphous portions of the material, which varies slightly with Ω. An adequate fit was obtained using the Lorentz distribution in combination with a linear background, using the fit equation given in Equation 1.

Figure 9 shows the resulting information obtained by fitting the normalized stacking peak data for TP-I-DOX-AL using Equation 1, as illustrated in Figure 10. The amplitude of the Lorentzian distribution (black) is less than 8×10^3 counts for $\Omega < 40°$, and increases quickly once the rotation angle passes 50°, as anticipated if the stacks of TAPPy-PDA molecules are organized so that the molecules lie predominantly in the plane of the film. The FWHM of the distribution (red) is essentially independent of Ω, indicating that the tactoid thickness is not a function of rotation angle. Finally, d_{001}, the average distance between 2DP molecules in the stack, shows some variation until Ω = 85°, at which point is constant at 3.744 Å, very close to the value of 3.846 Å reported by Natraj et al.[13] Rotating past 90° does not cause significant changes in FHWM or d_{001}, but amplitude does increase, suggesting a slight misalignment of the film relative to the incident X-ray beam.

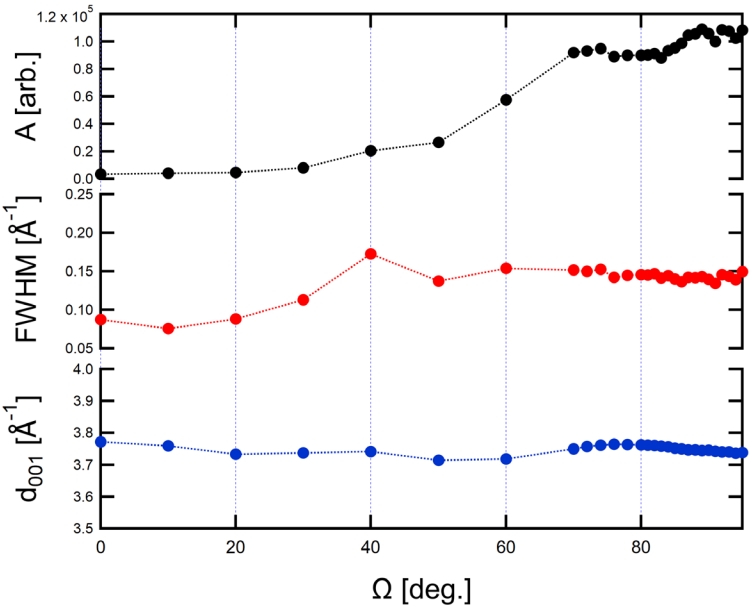

Figure 9. Amplitude (black), FWHM (red), and d_{001} (blue) as functions of Ω obtained from analysis of the normalized stacking peak for TP-I-DOX-AL.

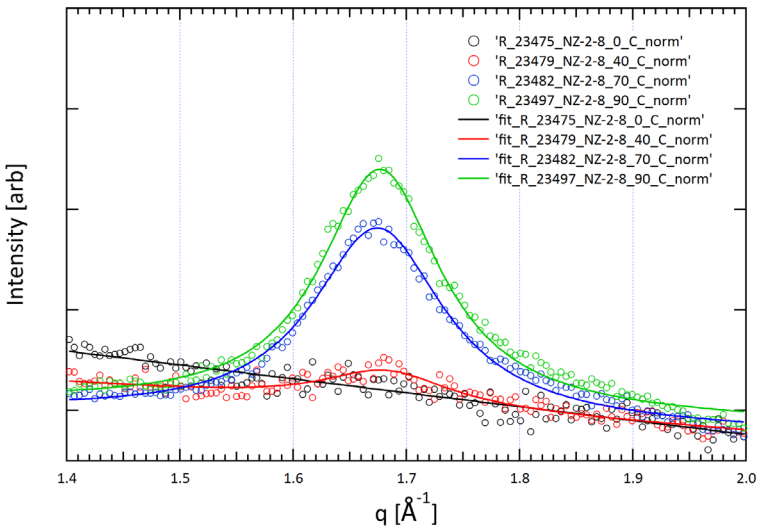

Figure 10. X-ray data for the stacking peak in TP-I-DOX-AL at various Ω, and the resulting fit of a Lorentz peak and linear background function (solid lines) to each dataset.

Another important characteristic is the degree of variation in the orientation of the TAPPy-PDA molecular sheets. To determine the "degree of orientation" in these materials, f was calculated for the stacking peak reflection as a function of azimuthal angle (Ψ). As illustrated in Figure 11A, the intensity of the stacking peak reflection was calculated as a function of Ψ for an annulus centered at 1.68 $Å^{-1}$ (red dashed line) with a width of ±0.1 $Å^{-1}$. Figure 11B shows the resulting 1D intensity data and a Gaussian distribution fit to the data as a part of the orientation function calculation.

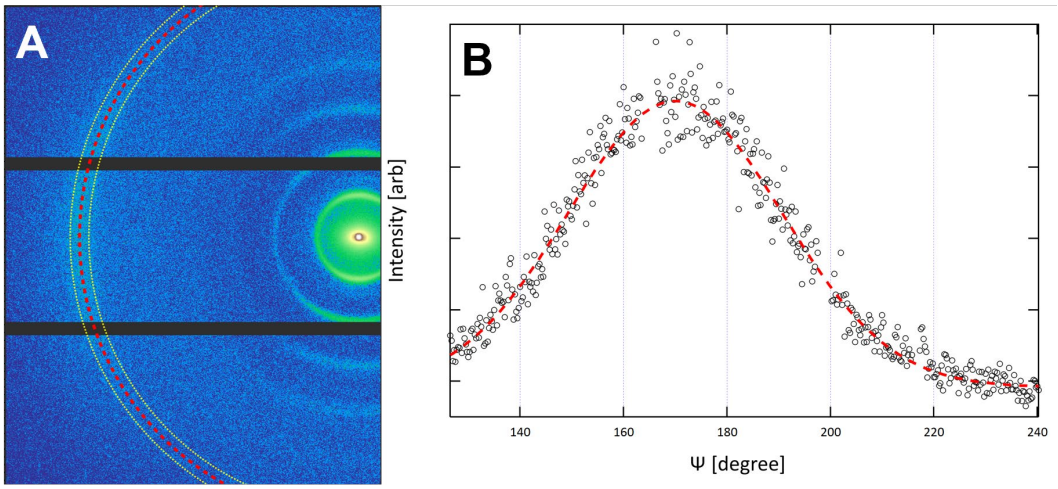

Figure 11. 2D scattering data (A) for TP-I-DOX-AL at Ω = 60° showing the circular window in which the intensity of the scattering peak was calculated as a function of Ψ, and (B) the corresponding 1D intensity data as a function of Ψ and the fit (red dashed line) to the data from which f was calculated.

This process was repeated for each dataset from Ω = 40° to 100°, and the resulting values of f are given in Figure 12. The average orientation value from 70° to 100° was 0.5674, indicating that the TAPPy-PDA sheets are well-aligned on a macroscopic level. The value of f is not expected to vary with changes in Ω.

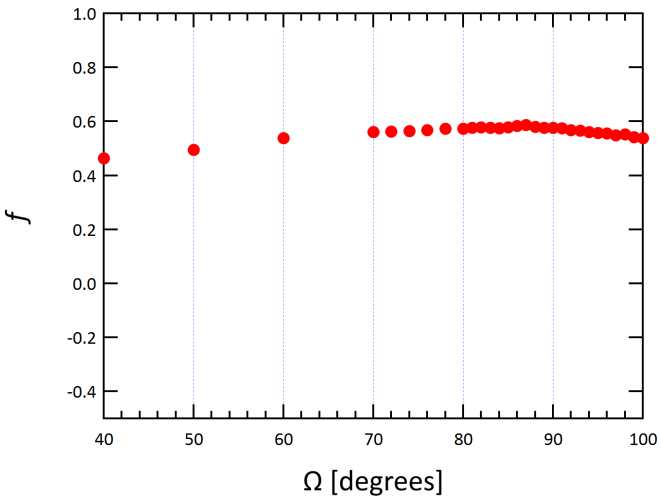

Figure 12. Values of the orientation parameter, *f*, as a function of Ω, for TP-I-DOX-AL.

Figure 13 shows the azimuthally averaged X-ray diffraction data collected from sample TP-I-THF-GR at rotation angles from Ω = 0° to 90°. As with TP-I-DOX-AL, the data have been normalized by the measured intensity in the power law region (q < 0.16 Å^{-1}) to reduce the effect of varying sample volume on measured intensity. Diffraction peaks from the TAPPy-PDA monoclinic crystal structure are clearly visible between 0.2 and 1.5 Å^{-1}, while the stacking peak is visible at approximately 1.68 Å^{-1}. The intensity of the stacking peak increases as the film is rotated up to Ω = 90°.

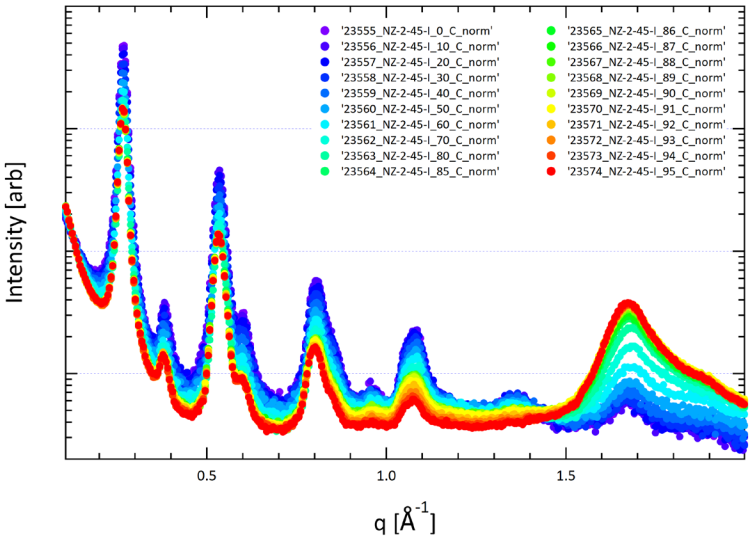

Figure 13. Azimuthally averaged 1D WAXS data for sample TP-I-THF-GR at various angles as noted, after normalizing the data to the power law region between 0.1 and 0.16 Å^{-1}.

For sample TP-I-THF-GR, the solution of TAPPy and PDA monomers was cast onto the surface of graphite. Close inspection of the high-q region including the stacking peak reveals the presence of an additional scattering feature. This additional scattering can be fit fairly well with a second Lorentzian distribution using Equation 1. An example is shown in Figure 14 of fitting the data for TP-I-THF-GR at $\Omega = 90°$. The interlayer spacing for graphite is 3.355 Å, corresponding to $q = 1.87$ Å^{-1}.[16] The graphite interlayer peak position from the fit in Figure 14 is 1.85 Å^{-1}, well within error given the simplicity of the fitting model and potential for systematic measurement errors.

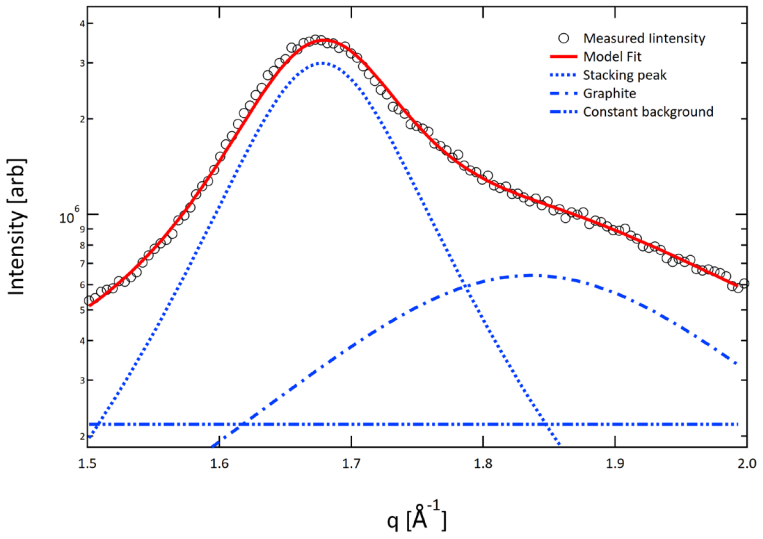

Figure 14. Representative fit of two Lorentz distributions and a constant background to the high-q scattering for TP-I-THF-GR. The diffraction maximum centered at 1.85 Å^{-1} is attributed to residual graphite from the substrate.

Figure 15 shows the intensity of the TP-I-THF-GR stacking peak as a function of Ψ, for all values of Ω measured, from which the Herman's orientation parameter was determined. The mean value of f for Ω between 85° and 95° was 0.640, with a standard deviation of 0.005°.

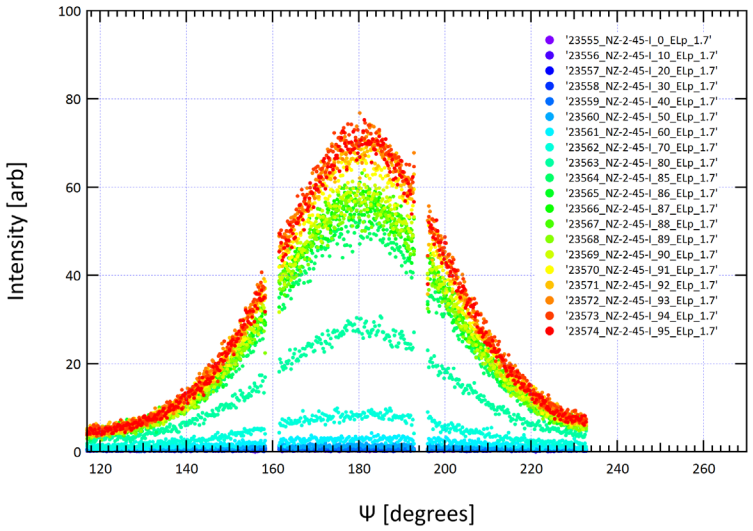

Figure 15. Stacking peak intensity as a function of azimuthal angle for TP-I-THF-GR.

The processes of data normalization, determining stacking peak location, and determining the degree of orientation indicated by the stacking peak was repeated for the remaining datasets. The 1D diffraction data after normalization and the 1D diffraction data in the vicinity of the stacking peak are given for each sample in the Appendix. The results of the analysis for all six samples are given in Table 2.

Table 2. Interplanar distance (d_{001}), orientation index (f), and their standard deviations (σ) for the stacking peak, (001), calculated for Ω ranging from 85° to 95°.

Sample	d_{001} (Å)	f
TP-I-DOX-AL	3.742 ± 0.004	0.573 ± 0.009
TP-I-DOX-GR	3.767 ± 0.003	0.655 ± 0.007
TP-I-THF-GR	3.748 ± 0.002	0.640 ± 0.005
TP-A-DOX-FP	3.73 ± 0.02	0.568 ± 0.006
TP-A-DOX-GR	3.770 ± 0.009	0.483 ± 0.004
TP-A-THF-GR	3.774 ± 0.004	0.482 ± 0.004

3.3 Grain Size Analysis

Using the Scherrer equation, the scattering data allow the estimation of the sizes of individual "grains" within the bulk 2D polymer, based on the diffraction peak position and the peak width at half of the maximum intensity (β) as described in Equation 2. An infinite, perfectly ordered crystal will have a value of β that is vanishingly small. As crystal size decreases, the limited crystal size leads to broadening of the diffraction peaks. Using the peak position and peak width data determined for the primary diffraction peak, (110), and the stacking peak, (001), lateral dimensions were calculated. As found previously for TAPB-PDA, the TAPPy-PDA COFs form stacks of 2D polymer that are much broader in the in-

plane direction than they are tall in the stacking direction. The aspect ratios of stack width to stack height are also given in Figure 16.

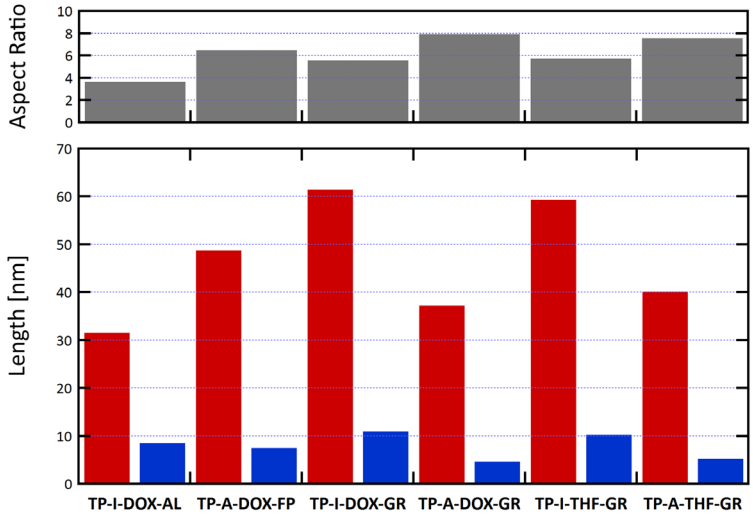

Figure 16. Grain dimensions calculated from the primary diffraction peak (width, in red) and the stacking peak (thickness, in blue) using the Scherrer equation. The ratio of the two dimensions is given above (gray).

4. Discussion

The goal of this study was to test the hypothesis that bulk films of oriented 2DP could be fabricated by casting dispersions of preformed 2DP flakes onto various substrates. The first step in the morphological analysis of these materials was to assess the structure of the 2DP lattice itself. The WAXS data in Figure 6 confirm the formation of the expected monoclinic structure with C2/*m* symmetry and dimensions in agreement with those published by Natraj et al., except as noted above.[13] The WAXS data in Figure 6 also suggests that the imine-functionalized materials are highly organized, with diffraction peaks up to (660) visible for samples TP-I-DOX-GR and TP-I-THF-GR. Samples TP-I-DOX-AL and TP-A-DOX-FP both are organized sufficiently well that the (440) diffraction maxima is observed. The samples having the least organized 2DP structure are TP-A-DOX-GR and TP-A-THF-GR, but even these samples exhibit higher order diffraction peaks up to the (330) reflection.

Close inspection of the high-*q* region ($q > 1.5$ Å^{-1}) of the data in Figure 6 shows little or no evidence of 2DP stacking. However, rotation of the samples about the *z*-axis caused the stacking peak to emerge as the rotation angle approached 90°, as illustrated in Figure 7. As shown in Figure 8, Figure 13, and the Appendix, all the samples exhibited this behavior. Observation of the stacking when the sample is rotated to high Ω but not when $\Omega = 0°$ proves that the feature giving rise to the

stacking peak, i.e., the stacking of individual 2DP molecules one on top of another, is anisotropic throughout the bulk of the sample. If individual stacks were present with random stack orientations, the stacking peak would be visible at all rotation angles, such as in a powder diffraction pattern. These data show that the individual stacks all have the same orientation, and that orientation is with the 2DP molecules aligned with the plane of the bulk film.

If the stacking peak is viewed as a (001) diffraction maximum from the TAPPy-PDA crystal structure, information about the relative degree of orientation of the crystallites can be quantified by calculating the Herman's orientation parameter, f. As shown in Figure 12, f is constant with Ω for TP-I-DOX-AL. More importantly, as shown in Table 2, all the films have orientation values around 0.55, with a maximum of 0.655 for TP-I-DOX-GR, and a minimum of 0.482 for TP-A-THF-GR. In general, the imine-functionalized TAPPy-PDA molecules seem to form better oriented stacks than the amide-functionalized TAPPy-PDA 2DPs.

The overall dimensions of the grains were estimated using the Scherrer equation (Equation 2) and presented in Figure 16. For all samples in this study, the 2DP grains are significantly larger in the direction parallel to the bulk film than in the direction normal to the bulk film (and 2DP molecules). As shown in Figure 16, aspect ratios range from 3.7 for TP-I-DOX-AL to 7.9 for TP-A-DOX-GR. In general, amide-functionalized 2DP films all have grains with higher aspect ratios than any of the imine-functionalized 2DP films. However, both TP-I-DOX-GR and TP-I-THF-GR both have the largest grain sizes in the lateral dimensions, at 61.5 nm and 59.4 nm. In general, one might characterize the samples by noting that the imine-functionalized 2DPs tend to comprise tall stacks of large molecules (low aspect ratio), while the amine-functionalized 2DPs comprise on average very low stacks of moderately sized 2DP molecules (higher aspect ratio). This difference may be caused by the chemical process used to convert imine functional groups to amide functional groups. That process may degrade the overall degree of polymerization of the 2DPs.

5. Conclusions

In this study, the effects of chemical functionality, solvent, and casting substrate on the alignment of 2DPs in bulk films were studied. COF molecules were polymerized from TAPPy and PDA monomers, precipitated from solution, and dried using supercritical CO_2. A portion of the resulting flakey powder was then subjected to a harsh chemical reaction that converted the imine functional groups to amide functional groups and then precipitated and dried a second time. The

resulting -imine and -amide 2DPs were then dispersed in either THF or dioxane and then cast onto various substrates.

Analysis of the resulting bulk films by X-ray scattering methods revealed that in all cases, the bulk film morphologies were those of TAPPy-PDA tactoids oriented such that the 2DP molecules lay parallel to the bulk substrate surface, a remarkable finding. When characterized with the incident X-ray beam normal to the bulk films, no evidence of stacking was observed. When the sample was rotated so that the X-ray beam angle of incidence decreased to 0 and the X-ray beam was parallel to the film, the scattering from the TAPPy-PDA lattice structure decreased and scattering from the stack of 2DP molecules increased dramatically. This combination confirms that the film morphology is one of 2DP tactoids, comprising many 2DP molecules stacked together, with the 2DP molecules lying in the plane of the bulk film.

Additional analysis of the scattering data indicates that there is a morphological distinction between the imine-functionalized and amide-functionalized materials. With the exception of the imine-functionalized 2DP cast on aluminum, the imine-functionalized 2DPs appear to form larger tactoids than those formed by the amide-functionalized materials. Conversely, the amide-functionalized 2DPs form tactoids that have a slightly higher aspect ratios than those formed by the imine-functionalized 2DPs. Given the small number of samples, the variation in solubility of the different 2DPs in dioxane and THF, these differences should not be considered conclusive.

6. References

1. Ding SY, Wang W. Covalent organic frameworks (COFs): from design to applications. Chem Soc Rev. 2013;42(2):548–568.
2. Geng KY et al. Covalent organic frameworks: design, synthesis, and functions. Chem Rev. 2020;120(16):8814–8933.
3. Evans AM et al. Two-dimensional polymers and polymerizations. Chem Rev. 2022;122(1):442–564.
4. Kingery WD, Bowen HK, Uhlmann DR. Introduction to ceramics. 2nd ed. Wiley-Interscience; 1976.
5. Black DR, Windover D, Henins A, Filliben J, Cline JP. Certification of standard reference material 660B. Powder Diffr. 2011;26(2):155–158.
6. Ilavsky J, Jemian PR. Irena: tool suite for modeling and analysis of small-angle scattering. J Appl Crystallogr. 2009;42:347–353.
7. Ilavsky J. Nika: software for two-dimensional data reduction. J Appl Crystallogr. 2012;45:324–328.
8. Pauw BR. Everything SAXS: small-angle scattering pattern collection and correction. J Phys Condens Matter. 2013;25(38):383201.
9. Cullity BD. Elements of X-ray diffraction. 2nd ed. Addison-Wesley series in metallurgy and materials. Addison-Wesley Publishing Company, Inc.; 1978.
10. Momma K, Izumi F. VESTA 3 for three-dimensional visualization of crystal, volumetric and morphology data. J Appl Crystallogr. 2011;44:1272–1276.
11. Patterson AL. The Scherrer formula for X-ray particle size determination. Phys Rev. 1939;56(10):978–982.
12. Roe R-J. Methods of X-ray and neutron scattering in polymer science. Oxford University Press; 2000.
13. Natraj A et al. Single-crystalline imine-linked two-dimensional covalent organic frameworks separate benzene and cyclohexane efficiently. J Am Chem Soc. 2022;144(43):19813–19824.
14. Li T, Senesi AJ, Lee B. Small angle X-ray scattering for nanoparticle research. Chem Rev. 2016;116(18):11128–11180.

15. Beyer FL, Sandoz-Rosado EJ, McLeod DC, Walck SD, Wetzel ED. Morphology of bulk two-dimensional polymer films. DEVCOM Army Research Laboratory (US); 2023. Report No.: ARL-TR-9765.

16. Howe JY, Rawn CJ, Jones LE, Ow H. Improved crystallographic data for graphite. Powder Diffr. 2003;18(2):150–154.

Appendix. X-ray Scattering Data

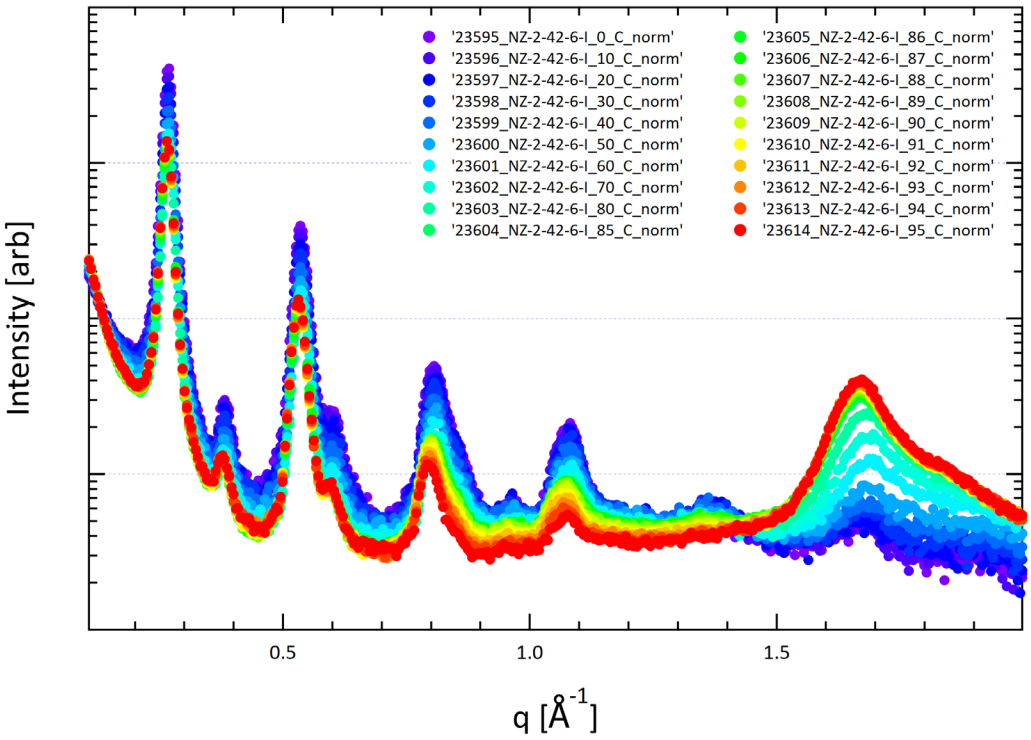

Figure A-1. Azimuthally averaged and normalized 1D X-ray diffraction data for sample TP-I-DOX-GR measured at different rotation angles.

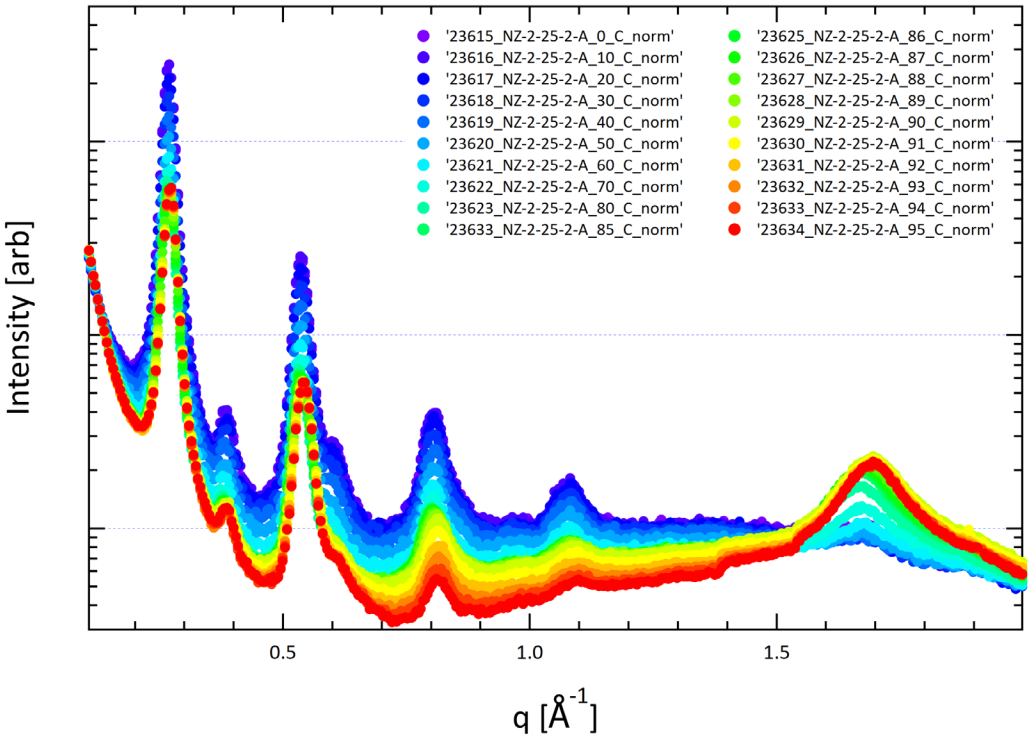

Figure A-2. Azimuthally averaged and normalized 1D X-ray diffraction data for sample TP-A-DOX-FP measured at different rotation angles.

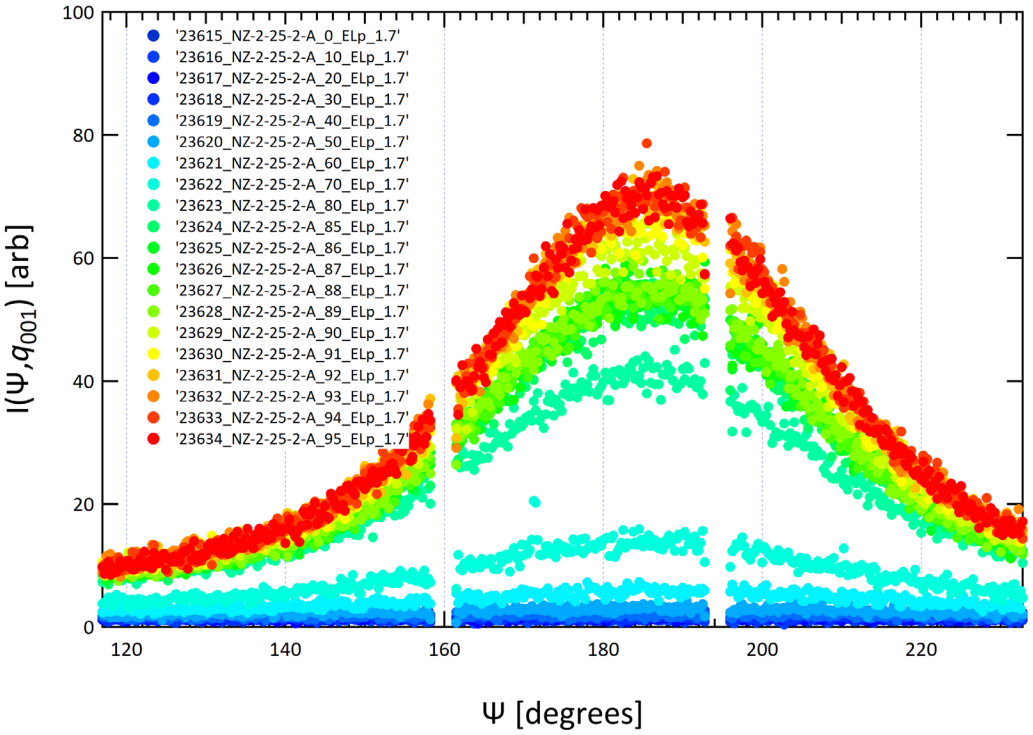

Figure A-3. Intensity as a function of azimuthal angle for the stacking peak of TP-A-DOX-FP measured at different rotation angles.

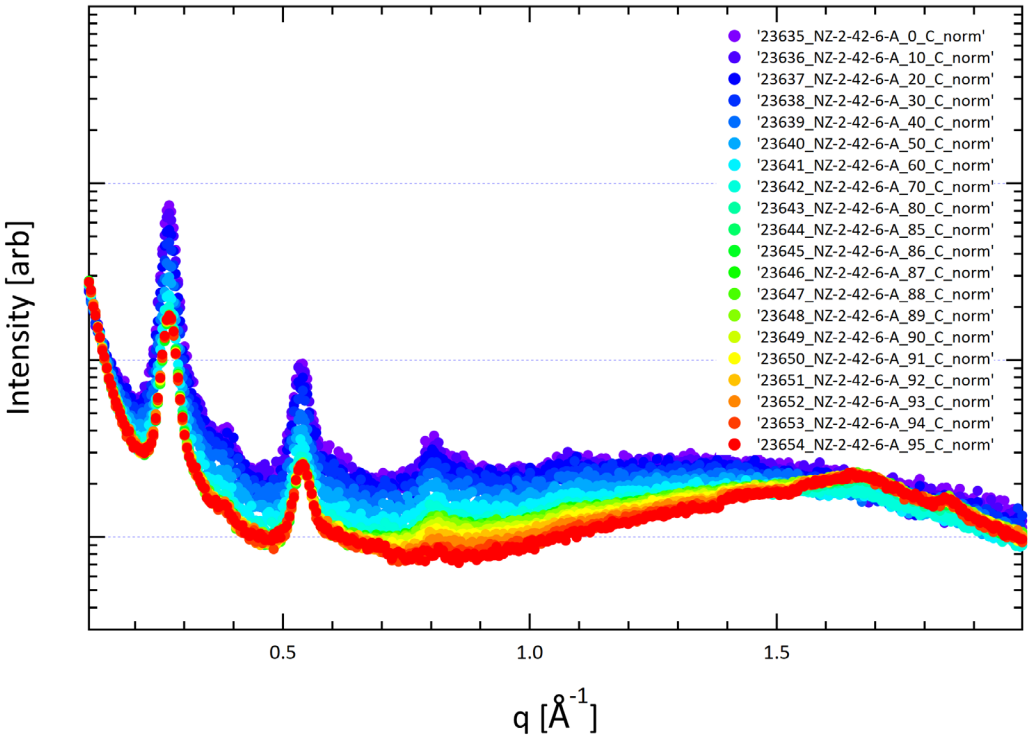

Figure A-4. Azimuthally averaged and normalized 1D X-ray diffraction data for TP-A-DOX-GR measured at different rotation angles.

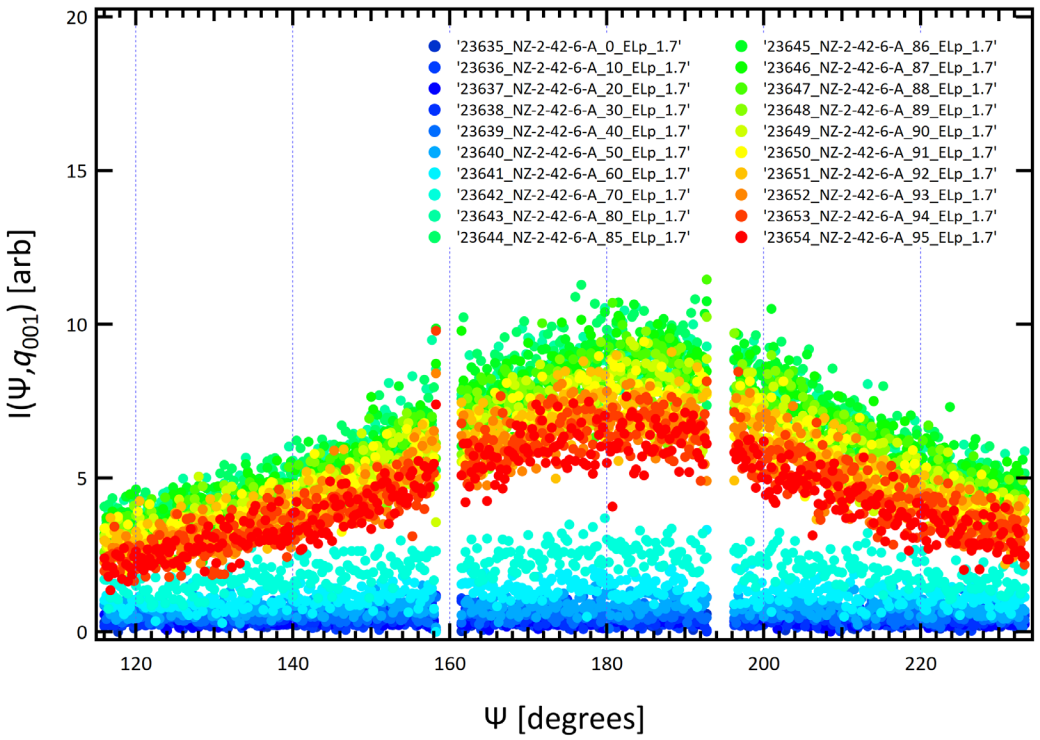

Figure A-5. Intensity of the stacking peak as a function of azimuthal angle for sample TP-A-DOX-GR measured at different rotation angles.

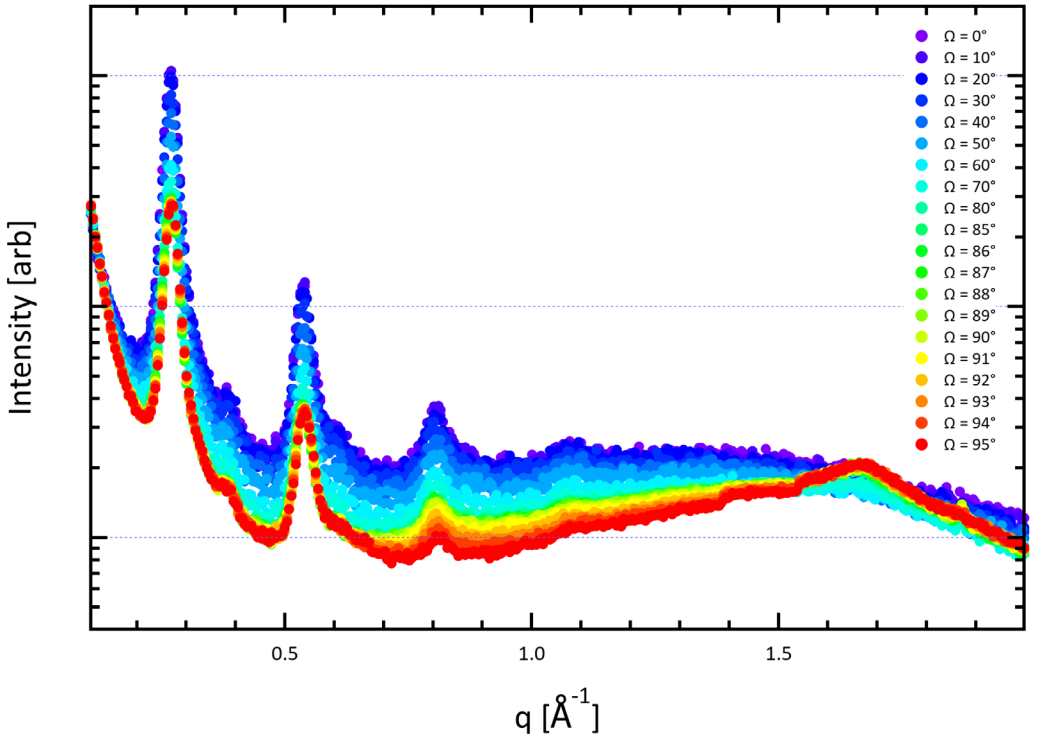

Figure A-6. Azimuthally averaged and normalized X-ray diffraction data for TP-A-THF-GR measured at different rotation angles.

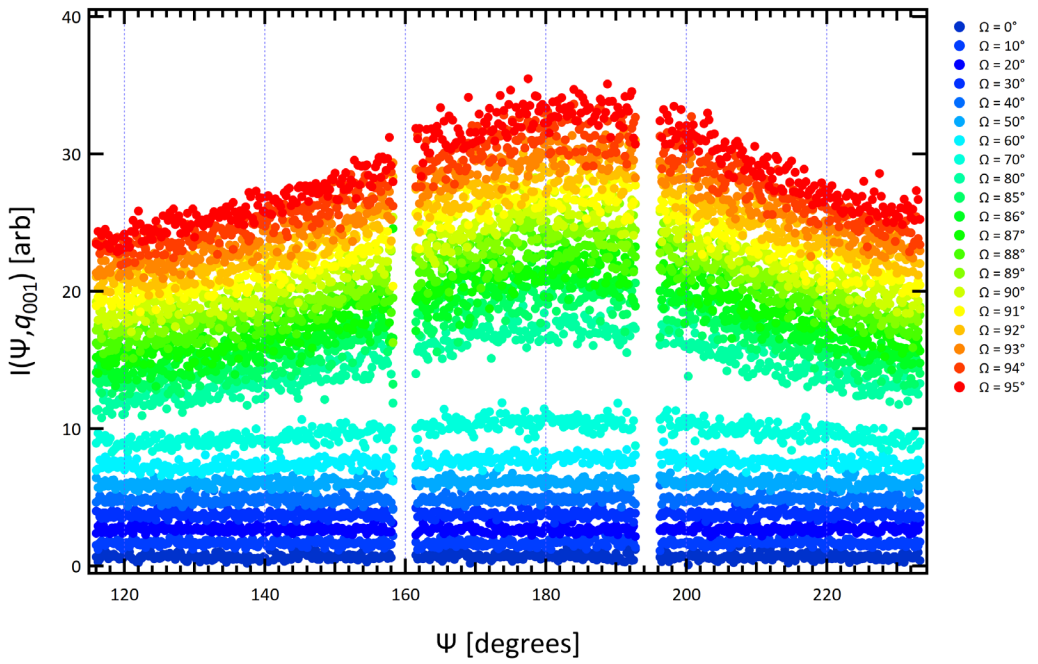

Figure A-7. Intensity as a function of azimuthal angle (ψ) for the stacking peak of TP-A-THF-GR measured at different rotation angles.

List of Symbols, Abbreviations, and Acronyms

1/2D	One-/Two-Dimensional
2DP	Two-Dimensional Polymer
A_i	Amplitude of Peak i
a, b, c	Crystallographic Unit Cell Dimensions
Al	Aluminum
ARL	Army Research Laboratory
CO_2	Carbon Dioxide
COF	Covalent Organic Framework
DEVCOM	U.S. Army Combat Capabilities Development Command
DMF	N,N-Dimethylformamide
f	Herman's Orientation Parameter
FWHM	Full-Width at Half-Maximum
I_0	Constant Background Intensity
h, k, l	Miller Indices defining Specific Crystallographic Planes
K	Scherrer Equation Constant
m	Slope of the Linear Background
n	Any Integer
NIST	National Institute of Standards and Technology
p	Power Law Exponent for Low-Angle Scattering
PDA	Terephthalaldehyde
$P(q)$	X-ray Scattering Form Factor
SAXS	Small-Angle X-ray Scattering
$S(q)$	X-ray Scattering Structure Factor
q	Magnitude of the Reciprocal Scattering Vector
q_i	Center of Peak i
TAPPy	1,3,6,8-Tetrakis(4-Aminophenyl)Pyrene

THF	Tetrahydrofuran
WAXS	Wide-Angle X-ray Scattering
x, y, z	Laboratory and Instrument Horizontal, Incident Beam, and Vertical Axes
α	Crystallographic Unit Cell Angle Between the b and c Axes
β	Crystallographic Unit Cell Angle Between the a and c Axes
β	Diffraction Peak Full-Width at Half-Maximum
γ	Crystallographic Unit Cell Angle Between the a and b Axes
γ_i	Half-Width at Half-Maximum of Peak i
θ	Diffraction Peak Bragg Angle, One-Half the Scattering Angle
λ	X-ray Wavelength
σ_i	Standard Deviation of Parameter i
τ	Grain Size
φ	Angle Between desired Orientation and Observed Orientation
Ψ	Azimuthal Angle
Ω	Angle of Sample Rotation about the z-Axis

1 (PDF)	DEFENSE TECHNICAL INFORMATION CTR DTIC OCA
1 (PDF)	DEVCOM ARL FCDD RLB CB TECH LIB